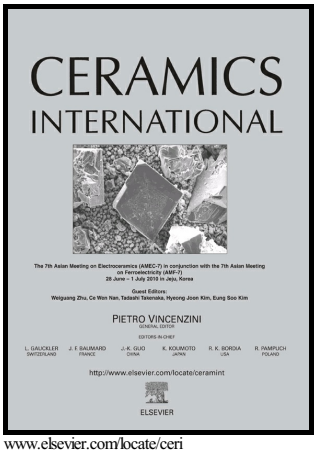

www.elsevier.com/locate/ceri

Influence of mechanical activation on functional properties of barium hexaferrite ceramics

D. Kosanović, V.A. Blagojević, A. Maričić, S. Aleksić, V.P. Pavlović, V.B. Pavlović, B. Vlahović

PII: S0272-8842(18)30091-9
DOI: https://doi.org/10.1016/j.ceramint.2018.01.078
Reference: CERI17210

To appear in: *Ceramics International*

Received date: 17 November 2017
Revised date: 10 January 2018
Accepted date: 10 January 2018

Cite this article as: D. Kosanović, V.A. Blagojević, A. Maričić, S. Aleksić, V.P. Pavlović, V.B. Pavlović and B. Vlahović, Influence of mechanical activation on functional properties of barium hexaferrite ceramics, *Ceramics International,* https://doi.org/10.1016/j.ceramint.2018.01.078

Influence of mechanical activation on functional properties of barium hexaferrite ceramics

D. Kosanović[a,*], V. A. Blagojević[a], A. Maričić[b], S. Aleksić[b], V. P. Pavlović[c], V. B. Pavlović[a], B. Vlahović[d,e]

[a]Institute of Technical Sciences of the Serbian Academy of Sciences and Arts, Knez Mihailova 35/IV, 11000 Belgrade, Serbia

[b]Joint Laboratory for Advanced Materials of SASA, Section for Amorphous Systems, Faculty of Technical Sciences Čačak, University of Kragujevac, Svetog Save 65, 32 000 Čačak, Serbia

[c]Faculty of Mechanical Engineering, University of Belgrade, Kraljice Marije 16, 11120 Belgrade, Serbia

[d]North Carolina Central University, Durham, NC, USA

[e]NASA University Research Center for Aerospace Device Research and Education and NSF Center of Research Excellence in Science and Technology Computational Center for Fundamental and Applied Science and Education, North Carolina, USA

Abstract

Barium hexaferrite ceramics were prepared using mechanically activated mixtures of iron and barium titanate. The 60:40 mass% Fe:$BaTiO_3$ powder mixtures were mechanically activated for different times (100-240 min) and sintered at 1100 and 1200 ^oC in order to determine the influence of mechanical activation of the precursor on the magnetic and dielectric properties of the resulting barium hexaferrite ceramics. The final product contained 84-89 mass% of $Ba_2Fe_{22.46}O_{38}Ti_{1.54}$ phase, with higher content corresponding to longer mechanical activation of the precursor. XRD and Raman measurements indicated that the remainder of the sample consists of leftover $BaTiO_3$ and hematite, which was formed by the oxidation of iron during mechanical activation and sintering in air. Magnetic properties of samples sintered at 1200 ^oC are superior to those sintered at 1100 ^oC, which can be attributed to higher $Ba_2Fe_{22.46}O_{38}Ti_{1.54}$ phase content. The position of the Curie temperature in 350-420 ^oC temperature region is consistent with 0.8:1 ratio of Ti to Ba. Maximum magnetization was observed for samples activated for 120 min. Dielectric properties of samples sintered at 1200 ^oC showed a dependence on frequency, with a significant drop in relative permittivity with an increase in

frequency in the low-frequency region, and relatively constant values of relative permittivity in the high-frequency region. The tangent loss showed a decrease with increase in frequency, where peaks corresponding to the resonance of the electron hopping frequency with the external field were observed in the samples corresponding to the longer mechanical activation. Dielectric properties showed relatively small changes for samples activated longer than 150 min.

Keywords: A. Milling; A. Sintering; C. Magnetic properties; C. Electrical properties

*Corresponding author.
E-mail address: kosanovic.darko@gmail.com, (D. Kosanović)

1. Introduction

Multiferroics are a class of materials that exhibit more than one ferroic polarization [1-2]. Primarily, the term 'ferroic polarization' indicates spontaneous magnetization, spontaneous electric polarization or spontaneous strain, which is realized by the application of external magnetic fields, electric fields or mechanical stress below the characteristic temperature (i.e., Curie temperature) [3]. Multiferroic materials exhibiting coexistence of at least two ferroic orderings (ferroelectric, ferromagnetic or ferroelastic) have recently stimulated ever-increasing research interest for their potential technological applications in multifunctional devices, such as memories and sensors [4-6]. However, the natural multiferroic single-phase compounds are rare, and none of the existing single-phase materials combines large magnetization and polarization at room temperature [7-8].

$BaTiO_3$ has been the most extensively investigated lead-free ferroelectric material [9], it has been widely used in practical applications, and allows for easy incorporation of 3d and 4d transition metals as a substitute for the titanium atom to produce ferromagnetism [10]. Importantly, Fe (110) and $BaTiO_3$ (100) planes are a relatively close match in terms of lattice constants (a mismatch is only about 1.4%), which allows layer-by-layer epitaxial growth of $Fe/BaTiO_3$ multi-layers with no misfit dislocations. Mechanical activation is a well-established preparation route for various titanate based based electroceramics [11-17]. At higher Fe:Ba ratios, barium hexaferrite $BaFe_{12}O_{19}$, an M type hexagonal ferrite, is usually formed, which, like other ferrite materials, has been used as a permanent magnet for

electronic and microwave applications [18-22], due to its large uniaxial magnetic anisotropy [23].

A recent study has shown that co-doping of $BaTiO_3$ with Mn and Fe leads to depression of the phase transition temperature and improved magnetization results, producing room temperature ferromagnetic and ferroelectric phase [24, 25]. Substitution of up to 10% Ti with Fe atoms, in $BaTiO_3$, introduces ferroelectric properties into $BaTi_{1-x}Fe_xO_3$, with optimal magnetodielectric coefficient at x = 2.5% [26]. A study of grain size effects in $BaTi_{0.5}Fe_{0.5}O_3$ materials produced by mechanochemical synthesis has shown a strong correlation between microstructural features and ferromagnetic and ferroelectric properties. While the relatively weak ferromagnetic effect was obtained through Fe-doping [27], ferroelectric properties declined precipitously with an increase in Fe-content, largely due to large leakage current caused by increased concentration of oxygen vacancies [28]. A study of dielectric and magnetic properties of mechanochemically synthesized barium hexaferrite has shown that magnetic properties improved with increased milling time, while dielectric permittivity showed little change [29]. Epitaxial barium hexaferrite films deposited on 6H-SiC exhibited large remanence ratio along in-plane axis and low along the out-of-plane axis, showing promise for microwave application [30].

In this study, mechanical activation of Fe/$BaTiO_3$ (FBT) powder mixture (with a powder mixture of 60 mass% of iron (Fe) and 40 mass% of barium titanate ($BaTiO_3$)) was characterized with a particular focus on the dependence of its magnetic properties vs. milling time and annealing temperature.

2. Experimental procedure

The initial powder was the mechanical mixture of 60 mass% of Fe (Aldrich, St. Louis, MO, p.a. 99.99%) and 40 mass% of $BaTiO_3$ (Aldrich, St. Louis, MO, p.a. 99%). The powder mixture was activated in a planetary ball mill (Retsch PM 400) in the air for 100, 120, 150, 180, 210 and 240 min at 300 rev/min. Initial mixtures were ground in a zirconium-oxide container (volume 500 cm^3), together with balls of a 10 mm diameter (the ratio of powder and the ball was 1:20). The powder mixtures were dried and calcined at a temperature of 700 ^oC, for 2 h inside a chamber furnace, after milling.

The samples of the activated after which calcined FBT powders were pressed at 5 t/cm^2 (500 MPa). They were sintered in air in a laboratory chamber furnace (Electron) whose maximum temperature is 1600 ^oC. The samples were placed into the furnace and sintered at a

temperature of 1200 ^{o}C for 2 h. The heating rate was 10 ^{o}C/min, and when the furnace reached the temperature of 1200 ^{o}C, the pressed samples were sintered isothermally for 2 h.

The X-ray powder diffraction patterns were obtained using a Rigaku Ultima IV X-ray diffraction (XRD) instrument in thin film geometry with grazing incidence angle of 0.5°, using Ni-filtered CuKα radiation (λ = 1.54178 Å). Diffraction data were acquired over the scattering angle 2θ from 10° to 70° with a step of 0.05° and acquisition rate of 2°/min and obtained data were analyzed with PDXL 2 software. Rietveld analysis was performed with full refinement using GSAS II software package [31]. Obtained values of R_{wp} (weighted residual factor) varied from 5.6% to 11.3% and the Goodness of Fit indicator was GoF~1. The texture of individual crystalline phases, as a measure of the preferential orientation of any particular crystalline plane with respect to the other planes of the respective crystal phase, was determined using the following equation [32]:

$$T_x = I/((1/n)\sum I_i) \qquad (1)$$

where T_x is texture coefficient, I is the intensity of an individual reflection belonging to a particular crystal plane normalized against the intensity of that same reflection in a reference powder sample, and n is the total number of reflections of individual crystalline phase considered.

The morphology and microstructure of sintered FBT were analyzed using a Scanning Electron Microscope (SEM, JSM-6390 LV JEOL, 30kV) coupled with EDS (Oxford Instruments X-Max^{N}).

The non-polarized light scattering spectra of the powder compact samples, compacted at 5 t/cm^2 (500 MPa) on a hydraulic press, were obtained at room temperature using the 633 nm line of a He-Ne laser, with a power supply of 1 mW at the sintered FBT-S samples. Raman scattering was recorded using a LabRam HR Evolution spectrometer (Horiba Jobin Yvon), in a backscattering geometry. The scanning range was 100 – 1100 cm^{-1}, with an increment step of 0.2 cm^{-1}.

Thermomagnetic measurements in air were conducted by Faraday method, which presumes the influence of the non-homogenous magnetic field on the magnetic sample during heating [33]. The measurement sensitivity of the magnetic force was 10^{-7} N in the applied magnetic field with an intensity of H_{app} = 16 kA/m.

The relative dielectric permittivity $\varepsilon_r(\omega)$ of $BaFe_{12-x}Ti_xO_{19}$ was measured on disc samples using low-frequency impedance analyzer HP 4119A and high-frequency impedance analyzer HP 4191A. First, the real and the imaginary part of impedance Z (ω) of disc samples were measured using measuring mode of parallel RC circuit. The obtained data were then

used for calculating parallel capacitance $C_p(\omega)$ and parallel resistance $R_p(\omega)$. In the second step, the relative dielectric permittivity $\varepsilon_r(\omega)= \varepsilon_r'(\omega)+j\varepsilon_r''(\omega)$ was calculated using Cp and R_p.

3. Results and discussion

A powder mixture of Fe and $BaTiO_3$ was mechanically activated for different periods of time and then sintered at 1100 and 1200 ^oC. Pre-sintered samples contained a mixture of $BaTiO_3$, Fe and different iron oxide phases, which combined to form $Ba_2Fe_{22.46}O_{38}Ti_{1.54}$ phase during sintering. Mechanical activation of pre-sintered samples of less than 100 min had not produced any significant effect on the powder microstructure [34] and, therefore, those samples were not investigated in detail. XRD patterns of a sintered mechanically activated powder mixture of Fe and $BaTiO_3$ are shown in Figure 1. Rietveld analysis (Table 1 and Supplement) indicates that the dominant crystalline phase in all of these samples is $Ba_2Fe_{22.46}O_{38}Ti_{1.54}$ with 84-89 mass%. The secondary crystalline phase is leftover $BaTiO_3$, which accounts for 11-16 mass%. The formation of $Ba_2Fe_{22.46}O_{38}Ti_{1.54}$ phase can be correlated with mechanical activation in the air, which converts Fe powder to Fe_3O_4 and Fe_2O_3, allowing the formation of hexaferrite $Ba_2Fe_{22.46}O_{38}Ti_{1.54}$ phase during sintering. It could be expected that there is also some amount of iron oxides left in the sample, however, it appears these phases are below the XRD detection threshold. The non-activated sample does not show any significant difference compared to the sample activated for 100 min, therefore, it was not investigated further in particular detail. Mechanical activation of the precursors has an effect on microstructural parameters of the crystalline lattice of $Ba_2Fe_{22.46}O_{38}Ti_{1.54}$ phase after sintering, resulting, in general, in expansion along *a*- and *b*-axes and contraction along *c*-axis, an increase in lattice volume and a decrease in the average crystallite size. Overall, the average crystallite size is considerably larger than in the precursor powders. The lattice volume expansion is relatively small at less than 1% in all of the samples. In addition, the contribution of $Ba_2Fe_{22.46}O_{38}Ti_{1.54}$ phase increases with increased time of mechanical activation, which can be expected and correlated with increased free surface available for chemical reaction due to smaller crystallite size and an increased concentration of surface defects on prolonged mechanical activation [34] allowing for a more effective conversion of precursors. Samples sintered after longer mechanical activation also exhibit higher values of lattice strain, suggesting a higher concentration of lattice defects. Texture analysis (Figure 1) shows that the samples generally exhibit similar orientation and that the dominant planes in

all of the samples are (114) and (107), which have a higher iron content. Planes with higher barium content, like (110) and (317) are less represented.

Scanning electron microscope study of sintered samples mechanically activated before sintering at 1200 ^{o}C shows significant changes in morphology caused by mechanical activation before sintering (Figure 2). Sample activated for 100 minutes exhibits granular structure with grains of a few tens of nanometers to a few micrometers in diameter and is generally similar to the sample that was not mechanically activated. Further pre-sintering mechanical activation of 150 min causes the sintered grains to be much more consolidated and indicates that the sintering process has become more efficient as a result of mechanical activation. This is confirmed by further mechanical activation for 210 min, where the sample is even more compact and it is hard to identify individual grains. EDS analysis (Figure 3) shows that the sample that was mechanically activated for 210 minutes contains more oxygen than the samples activated for shorter periods of time, which is consistent with mechanical activation in the air, leading to the creation of defects and larger specific surface area in the pre-sintered sample. In addition, chemical mapping of the sample surface shows that pre-sintering mechanical activation leads to better phase separation, as shown in Figure 4, where Fe-rich and Ti-rich regions show an increasing degree of separation. This can be correlated with results of XRD phase composition, where the amount of $Ba_2Fe_{22.46}O_{38}Ti_{1.54}$ phase increased with increase in mechanical activation time. This suggests that the reduction in grain size by mechanical activation improves the homogeneity of the pre-sintered mixture and allows more efficient chemical reaction during sintering, providing both higher yield of $Ba_2Fe_{22.46}O_{38}Ti_{1.54}$ phase and a more compact sample.

Raman spectra in Figure 5 show that in all mechanically activated samples, the dominant signal comes from a barium hexaferrite phase, which can be attributed to $Ba_2Fe_{22.46}O_{38}Ti_{1.54}$ crystalline phase (marked with B in Figure 5 [35]). Hematite and $BaTiO_3$ are observed in relatively small amounts, with higher content in the samples activated for shorter times, which is consistent with XRD measurements. In the sample activated for 100 min, two strong hematite lines appear (224 and 293 cm^{-1}), with another line present as a shoulder around 493 cm^{-1} [36, 37]. In the same sample, $BaTiO_3$ manifests as a weak peak corresponding to superimposed E(3TO), E(2LO) and B1(1TO+1LO) modes, characteristic of tetragonal $BaTiO_3$. At longer activation times, distinct peaks corresponding to hematite and $BaTiO_3$ are not observed, but a weak peak corresponding to superimposed A_1(2TO) $BaTiO_3$ mode and the strongest hematite mode E_g around 292 cm^{-1}. The presence of the superimposed E(3TO), E(2LO) and B1(1TO+1LO) modes of tetragonal $BaTiO_3$ are observed

as a weak signal near barium hexaferrite peak at ~339 cm^{-1}. The peak around 525 cm^{-1} could also be attributed to the contribution of E(4TO) and A_1(3TO) modes of $BaTiO_3$, in addition to barium hexaferrite contribution. This behavior can be explained by the existence of non-reacted iron-oxide in the final product: phase analysis indicates 84-89% of $Ba_2Fe_{22.46}O_{38}Ti_{1.54}$ crystalline phase, with an increase in content with increase in the duration of mechanical activation. This is close to the theoretical maximum content of $Ba_2Fe_{22.46}O_{38}Ti_{1.54}$ phase for a fully reacted 60-40 mass% mixture of Fe and $BaTiO_3$ of around 93%, leaving estimated less than 2 mass% iron unreacted in the sample for the formation of iron-oxides. While the content of these iron oxides is most likely too small to detect in the XRD, it can easily accumulate locally on the surface of $Ba_2Fe_{22.46}O_{38}Ti_{1.54}$ grains and provide strong enough Raman signal to be observed in some of the samples.

Barium hexaferrite phases exhibit high electrical resistivity and a low magnetic loss, coupled with high magnetic anisotropy, high saturation magnetization and a high temperature of ferrimagnetic transition [38]. In pressed non-sintered samples, magnetization reaches a maximum value for mechanical activation for 100 min, due to the formation of magnetic iron oxides during mechanical activation in the air, in particular, Fe_3O_4 (Figure 6). The variations in values of magnetization for longer times of mechanical activation can be attributed to content variations of Fe_2O_3 and Fe_3O_4 in the sample. Samples sintered at 1100 and 1200^oC for 2h exhibit significantly lower values of magnetization, which originates from the formation of $Ba_2Fe_{22.46}O_{38}Ti_{1.54}$, which is identified as the dominant crystalline phase in the XRD and is not as good magnetic material as magnetite. Higher values of magnetization after sintering at 1200^oC, compared to sintering at 1100^oC, correspond to higher $Ba_2Fe_{22.46}O_{38}Ti_{1.54}$ content in these samples.

Figure 7 shows the temperature dependence of magnetization for a sample activated for 120 minutes and sintered at 1200 ^oC for 2 h. Magnetization drops about 20% at a temperature of around 100 ^oC, which corresponds to $BaTiO_3$ phase transformation and transition from ferroelectric tetragonal to paraelectric cubic phase. The sample exhibits Curie temperature in 350-420 ^oC temperature region, as indicated by the loss of magnetization. Pure $BaFe_{12}O_{19}$ exhibits a Curie temperature in 450-500 ^oC region, and values of 350-420 ^oC are roughly consistent with the presence of Ti at 0.8:1 ratio to Ba [39], which is consistent with the presence of $Ba_2Fe_{22.46}O_{38}Ti_{1.54}$ phase. When this sample was cooled outside of the magnetic field and then heated again, there was no significant change in magnetic properties and their temperature dependence. However, when the sample was cooled in a magnetic field with H = 16 kA/m, magnetization at temperatures close to room temperature was 3.5-4 times

higher than in the original sample. On the other side, this sample exhibited continuous loss of magnetization on heating, while Curie temperature remained the same. This increase in magnetization at room temperature was permanent and did not decay over time when the sample was removed from the magnetic field.

Dependence of dielectric properties on mechanical activation shows that mechanically activated samples exhibit a significant increase in both real and imaginary part of the dielectric permittivity (Figure 8). Dielectric permittivity decreases relatively sharply with increase in frequency, which can be explained by the existence of interfacial polarization based on the Maxwell-Wagner two-layer model [40, 41]. Since the ferrite grains are good conductors and grain boundaries are fairly poor conductors, the high values of the dielectric permittivity at low frequencies can be attributed to space charge polarization produced at the grain boundaries. At higher frequencies, electron hopping between Fe^{2+} and Fe^{3+} ions occurs at a lower frequency than the frequency of the external field, causing dispersion [42]. The real part of the dielectric permittivity remains relatively constant at higher frequencies, which is consistent with previous studies [29]. The high values of dielectric permittivity are consistent with those obtained for Mg and Ti-doped $BaFe_{12}O_{19}$ [39], where highest values were obtained for a system with 1:1:1 ratio of Ba:Ti:Mg.

Figure 9 shows that all of the systems exhibit relatively high values of tangent loss, with mechanically activated systems generally exhibiting some what higher values. Dielectric loss occurs when the polarization of the material lags behind the applied electric field and is typically caused by impurities and defects in the material. The energy required for electron exchange between Fe^{2+} and Fe^{3+} ions decreases with increase in frequency, leading to a general decrease of tangent loss with an increase in the frequency of the applied electric field. The peaks in the tangent loss dependence on frequency occur when the electron hopping frequency between Fe^{2+} and Fe^{3+} ions matches the frequency of the external field, and this effect appears to be the dominant factor in the amplitude of the tangent loss [39].

4. Conclusion

$BaTiO_3$ and iron powder mixture with 40:60 mass composition (14:86 atomic ratio of Ba:Fe) were mechanically activated and then sintered at 1100 and 1200 ^{o}C. The resulting samples contained mostly hexaferrite $Ba_2Fe_{22.46}O_{38}Ti_{1.54}$ phase and leftover $BaTiO_3$ and hematite, while the presence of leftover iron oxides could not be determined using XRD, although magnetic and Raman measurements indicated they were present in the sample. Samples

sintered at 1200 ^{o}C exhibited better magnetic properties than those sintered at 1100 ^{o}C, due to the higher content of hexaferrite phase. Maximum value of magnetization was observed for samples activated for 120 min. Dielectric properties showed dependence on frequency, where there was a significant drop in dielectric permittivity with an increase in frequency at low frequencies, while the real part of the dielectric permittivity remained relatively constant at high frequencies. The tangent loss showed a general decrease with increase in frequency, with peaks corresponding to the resonance of the electron hopping frequency with the external field occurring in samples with higher mechanical activation times. Dielectric properties show relatively little change for activation longer than 150 min. High observed values of dielectric permittivity are consistent with previously published work for similar systems.

Acknowledgments

This research was performed within the projects OI 172057, funded by the Ministry of Education, Science and Technological Development of the Republic of Serbia and the projects F/198, funded by the Serbian Academy of Sciences and Arts. This work is also supported by the NSF CREST (HRD-0833184), NASA (NNX09AV07A) and NSF-PREM (1523617) awards. The authors would like to thank academician M. M. Ristić for invaluable discussion and support during the writing of this paper.

References

[1] H. Schmid, Multi-ferroic magnetoelectrics, Ferroelectrics, 162 (1) (1994) 317-338.

[2] M. Fiebig, Revival of the magnetoelectric effect, J. Phys. D: Appl. Phys. 38 (2005) R123-R152.

[3] L. E. Cross, Ferroic Materials and composites: Past, present and future, Ch. 5 in "Advanced Ceramic III" Elsevier Applied Science, New York, 1998. Edited by S. Somiya.

[4] K. F. Wang, J. M. Liu, Z. F. Ren, Multiferroicity: the coupling between magnetic and polarization orders, Advances in Physics, 58 (4) (2009) 321-448.

[5] C. W. Nan, M. I. Bichurin, S. Dong, D. Viehland, G. Srinivasan, Multiferroic magnetoelectric composites: Historical perspective, status, and future directions, Journal of Applied Physics, 103 (3) (2008) 031101.

[6] J. F. Scott, Nat. Mater., Data storage: Multiferroic memories, 6 (2007) 256-257.

[7] Z. Li, Y. Wang, Y. Lin, C. Nan, Evidence for stress-mediated magnetoelectric coupling in multiferroic bilayer films from magnetic-field-dependent Raman scattering, Phys. Rev. B, 79 (2009) 180406.

[8] J. Wang, Y. Zhang, J. Ma, Y. Lin, C.W. Nan, Magnetoelectric behavior of $BaTiO_3$ films directly grown on $CoFe_2O_4$ ceramics, J. Appl. Phys., 104 (2008) 014101.

[9] S. K. Das, R. N. Mishra, B. K. Roul, Magnetic and ferroelectric properties of Ni doped $BaTiO_3$, Solid State Communications, 191 (2014) 19-24.

[10] V. Paunović, V. V. Mitić, M. Đorđević, M. Marjanović, Lj. Kocić, Electrical Characteristics of Er Doped $BaTiO_3$ Ceramics, Science of Sintering, 49 (2017) 129-137.

[11] S. Filipović, N. Obradović, V. B. Pavlović, D. Kosanović, M. Mitrić, N. Mitrović, V. Pouchly, M. Kachlik, and K. Maca, Advantages of Combined Sintering Compared to Conventional Sintering of Mechanically Activated Magnesium Titanate, Science of Sintering, 46 (3) (2014) 283-290.

[12] D. Kosanović, J. Živojinović, N. Obradović, V. P. Pavlović, V. B. Pavlović, A. Peleš, and M. M. Ristić, The Influence of Mechanical Activation on the Electrical Properties of $Ba_{0.77}Sr_{0.23}TiO_3$ Ceramics, Ceramics International, Vol. 40 (8 part A) (2014) 11883-11888.

[13] S. Filipović, N. Obradović, D. Kosanović, V. Pavlović, A. Djordjević, Sintering of the mechanically activated MgO-TiO_2 system, Journal of Ceramic Processing Research, 14 (1) (2013) 31-34.

[14] J. Živojinović, V. P. Pavlović, D. Kosanović, S. Marković, J. Krstić, V. A. Blagojević, V. B. Pavlović, The influence of mechanical activation on structural evolution of nanocrystalline $SrTiO_3$ powders, Journal of Alloys and Compounds, 695 (2017) 863-870.

[15] D. Kosanović, N. Obradović, J. Živojinović, S. Filipović, A. Maričić, V. Pavlović, Y. Tang, M. M. Ristić, Mechanical-Chemical Synthesis $Ba_{0.77}Sr_{0.23}TiO_3$, Science of Sintering 44, 1 (2012) 47-55.

[16] D. Kosanović, N. Obradović, J. Živojinović, A. Maričić, V. P. Pavlović, V. B. Pavlović, M. M. Ristić, The Influence of Mechanical Activation on Sintering Process of $BaCO_3$-$SrCO_3$-TiO_2 System, Science of Sintering, 44 (3) (2012) 271-280.

[17] N. Labus, Z. Z. Vasiljević, D. Vasiljević-Radović S. Rakić, M. V. Nikolić, Two Step Sintering of $ZnTiO_3$ Nanopowder, Science of Sintering, 49 (2017) 51-60.

[18] D. B. Hovis, K. T. Faber, Textured microstructures in barium hexaferrite by magnetic field assisted gelcasting and templated grain growth, Scripta Materialia, 44 (11) (2001) 2525-2529.

[19] R. Martinez Garcia, E. Reguera Ruiz, E. Estevez Rams, R. Martinez Sanchez, Efect of precursor milling on magnetic and structural properties of $BaFe_{12}O_{19}$ M-ferrite, Journal of Magnetism and Magnetic Materials, 223 (2001) 133-137.

[20] P. Shepherd, K. K. Mallick, R. J. Green, Magnetic and structural properties of M-type barium hexaferrite prepared by co-precipitation, Journal of Magnetism and Magnetic Materials, 311 (2007) 683-692.

[21] D. L. Sekulić, Z. Z. Lazarević, Č. D. Jovalekić, A. N. Milutinović, N. Z. Romčević, Impedance Spectroscopy of Nanocrystalline $MgFe_2O_4$ and $MnFe_2O_4$ Ferrite Ceramics: Effect of Grain Boundaries on the Electrical Properties, Science of Sintering, 48 (2016) 17-28.

[22] E.-Eromosele C. Osereme, I. B. Iserom, I. E. E. Joshua , Synthesis, Microstructure and Magnetic Properties of Nanocrystalline $MgFe_2O_4$ Particles: Effect of Mixture of Fuels and Sintering Temperature, Science of Sintering, 48 (2016) 221-235

[23] Smit J., Wijn, H. P. J., Ferrites. Philips' Technical Library, Eidenhoven, Chapter IX, 1959.

[24] S. Rajan, P. M. Mohammed Gazzali, G. Chandrasekaran, Electrical and magnetic phase transition studies of Fe and Mn co-doped $BaTiO_3$, Journal of Alloys and Compounds, 656 (2016) 98-109.

[25] L. Padilla-Campos, D. E. Diaz-Droguett, R. Lavín, S. Fuentes, Synthesis and structural analysis of Co-doped $BaTiO_3$, Journal of Molecular Structure, 1099 (2015) 502-509.

[26] A. Rani, J. Kolte, S. S. Vadla, P. Gopalan, Structural, electrical, magnetic and magnetoelectric properties of Fe doped $BaTiO_3$ ceramics, Ceramics International, 42 (2016) 8010-8016.

[27] Kuldeep Chand Verma, Vinay Gupta, Jaspreet Kaur, R. K. Kotnala, Raman spectra, photoluminescence, magnetism and magnetoelectric coupling in pure and Fe doped $BaTiO_3$ nanostructures, Journal of Alloys and Compounds, 578 (2013) 5-11.

[28] K. Samuvel, K. Ramachandran, Structure, electrical and magnetic property investigations on Fe-doped hexagonal $BaTiO_3$, Optik, 127 (2016) 1781-1786.

[29] W. S. Castro, R. R.Corrêa, P. I. Paulim Filho, J. M. Rivas Mercury, A. A. Cabrala, Dielectric and magnetic characterization of barium hexaferrite ceramics, Ceramics International, 41 (2015) 241-246.

[30] X. Zhang, Z. Yue, Y. Zhang, Structure characterization and magnetic properties of barium hexaferrite films deposited on 6H-SiC with random in-plane orientation, Ceramics International, 43 (2017) 8611-8615.

[31] B. H. Toby, R. B. Von Dreele, GSAS-II: the genesis of a modern open-source all-purpose crystallography software package, J. Appl. Crystallogr., 46 (2013) 544-549.

[32] G. B. Harris, X. Quantitative measurement of preferred orientation in rolled uranium bars, Philos. Mag., 43 (336) (1952) 113-123.

[33] Z. Ristanović, A. Kalezić-Glišović, N. Mitrović, S. Đukić, D. Kosanović, A. Maričić, The influence of mechanochemical activation and thermal treatment on magnetic properties of the $BaTiO_3$-Fe_xO_y powder mixture, Science of Sintering, 47 (1) (2015) 3-14.

[34] D. Kosanović, N. Obradović, V. P. Pavlović, S. Marković, A. Maričić, G. Rašić, B. Vlahović, V. B. Pavlović, M. M. Ristić, The influence of mechanical activation on the morphological changes of Fe/$BaTiO_3$ powder, Materials Science and Engineering B, 212 (2016) 89-95.

[35] F. M. S. Júnior, Carlos W. A. Paschoal, Spin-phonon coupling in $BaFe_{12}O_{19}$ M-type hexaferrite, J. Appl. Phys., 116 (2014) 244110.

[36] D. L. A. de Faria, S. V. Silva, M. T. de Oliveira, Raman microspectroscopy of some iron oxides and oxyhydroxides, Journal of Raman Spectroscopy, 28 (1997) 873-878.

[37] Y.-S. Li, J. S. Church, A. L. Woodhead, Infrared and Raman spectroscopic studies on iron oxide magnetic nanoparticles and their surface modifications, J. Magn. Magn. Mater., 324 (8) (2012) 1543-1550.

[38] Ü. Özgür, Y. Alivov, and H. Morkoç, Microwave ferrites, part 1: fundamental. Properties, J. Mater. Sci. Mater. Electron., 20 (9) (2009) 789-834.

[39] V. V. Soman, V. M. Nanoto, D. K. Kulkarni, Dielectric and magnetic properties of Mg–Ti substituted barium-hexaferrite, Ceramics International, 39 (2013) 5713-5723.

[40] C. G. Koops, On the dispersion of resistivity and dielectric constant of some semiconductors at audio frequencies, Physical Review, 83 (1951) 121-124.

[41] K. W. Wagner, The theory of imperfect dielectrics, Annals of Physics (Leipzig), 40 (1913) 817-855.

[42] S. A. Lokare, D. R. Patil, R. S. Devan, S. S. Chougale, Y. D. Kolekar, B. K. Chougale, Electrical conduction, dielectric behavior and magneto electric effect in (x)$BaTiO_3$ + (1-x)$Ni_{0.94}Co_{0.01}Mn_{0.05}Fe_2O_4$ ME composites, Materials Research Bulletin, 43(2008) 326-332.

Fig. 1. XRD patterns of samples of sintered mechanically activated powders (left); texture analysis (right).

Fig. 2. SEM images of samples mechanically activated for 100, 150 and 210 min.

Fig. 3. EDS spectra of samples mechanically activated for 100, 150 and 210 min.

Fig. 4. Chemical mapping of samples mechanically activated for 100, 150 and 210 min.

Fig. 5. Raman spectra of sintered mechanically activated Fe-$BaTiO_3$ powders (B – barium hexaferrite; H – hematite; BT – $BaTiO_3$).

Fig. 6. Dependence of magnetization on mechanical activation time in non-sintered samples (left) and samples sintered at 1100 and 1200°C (right).

Fig. 7. Temperature dependence of magnetization of a sample activated for 120 min and sintered at 1200°C for 2 h during two successive heating cycles (H = 16 kA/m, heating rate 20°C/min) when cooling was conducted in a magnetic field.

Fig. 8. Real (left) and imaginary (right) part of the dielectric permittivity of mechanically activated samples sintered at 1200°C for 2 h.

Fig. 9. Tangent loss of mechanically activated samples sintered at 1200°C for 2 h.

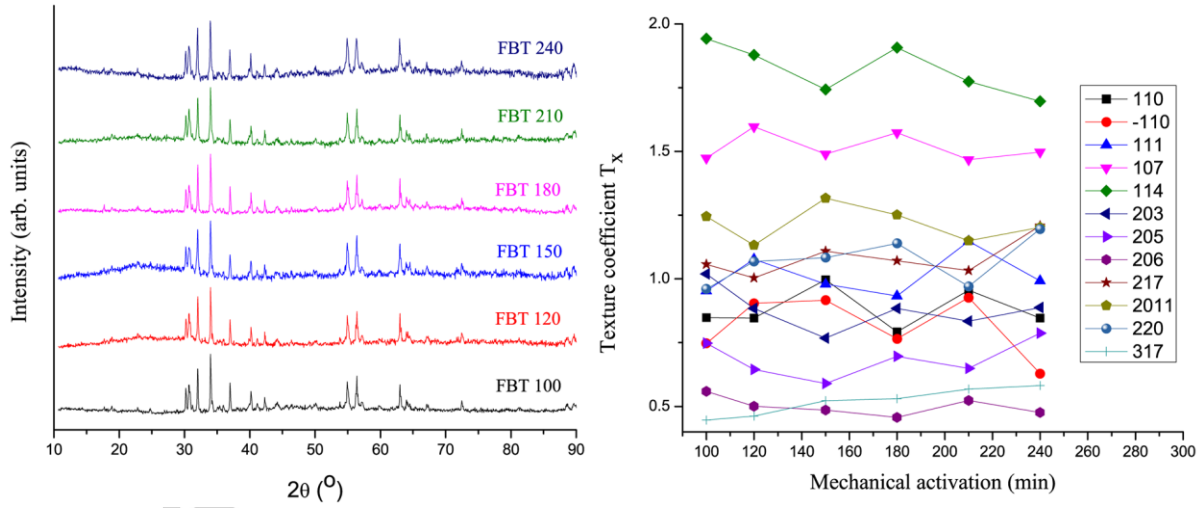

Fig. 1

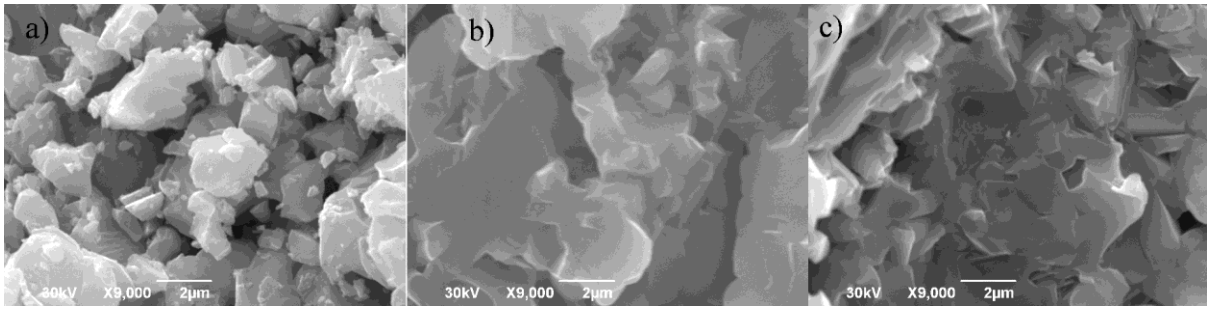

Fig. 2

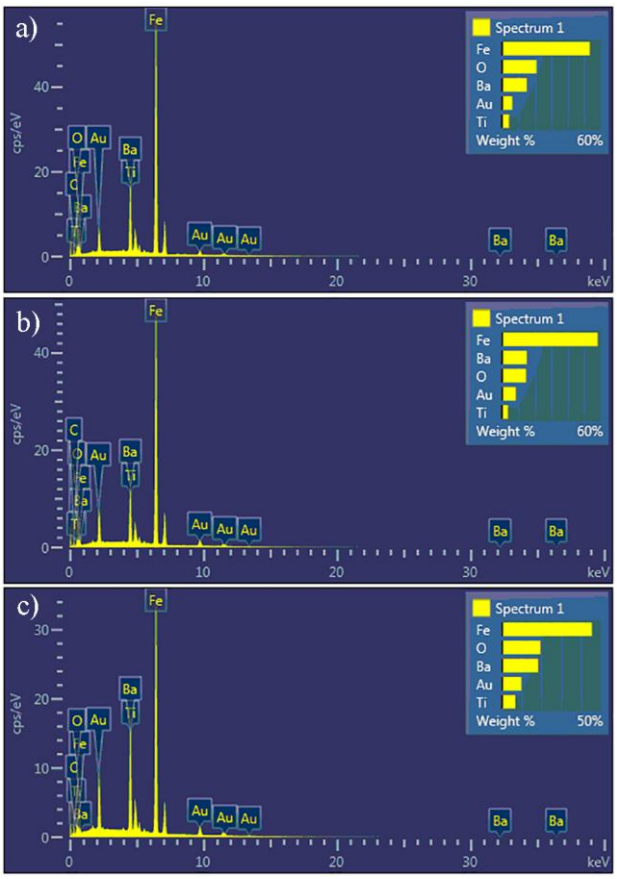

Fig. 3

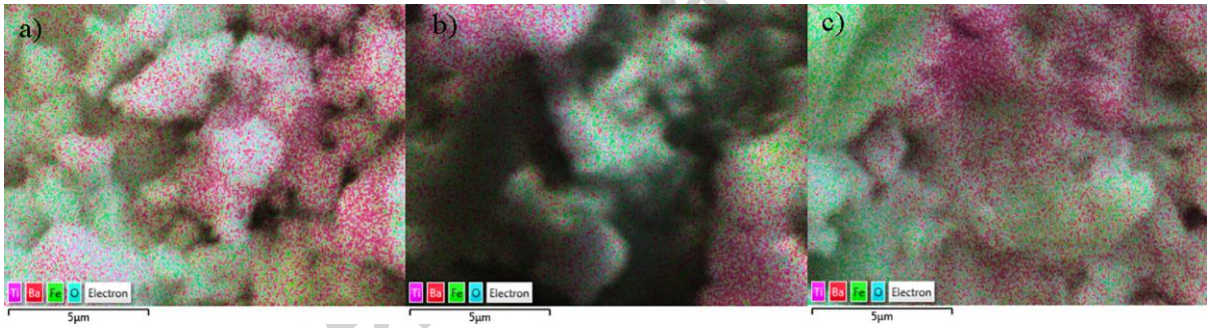

Fig. 4

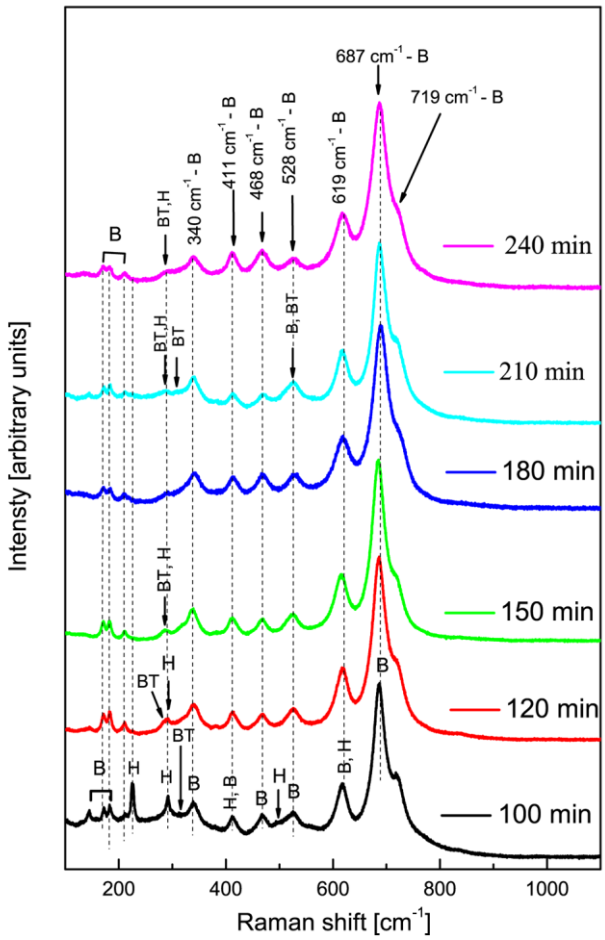

Fig. 5

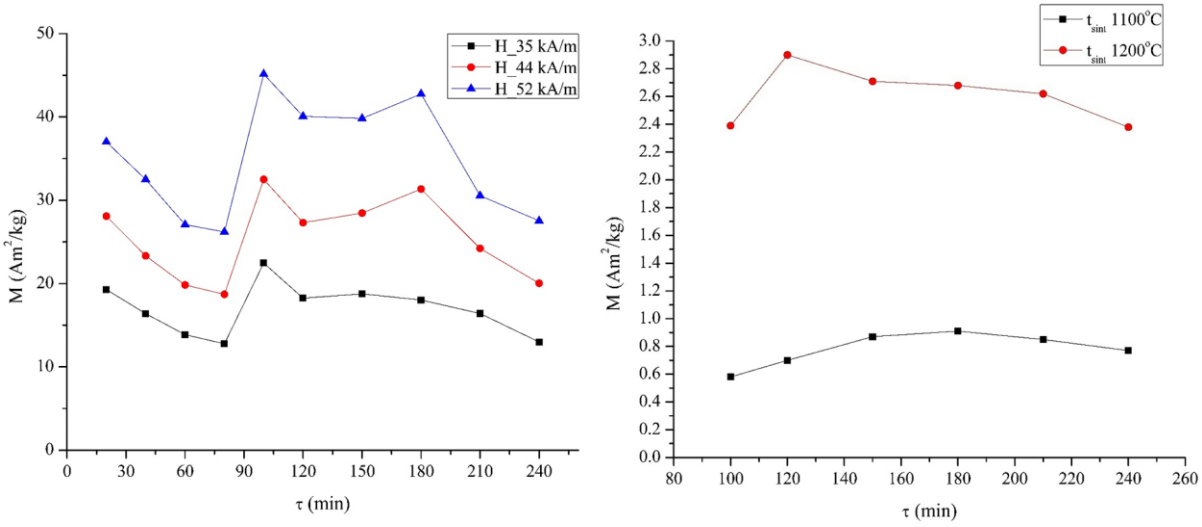

Fig. 6

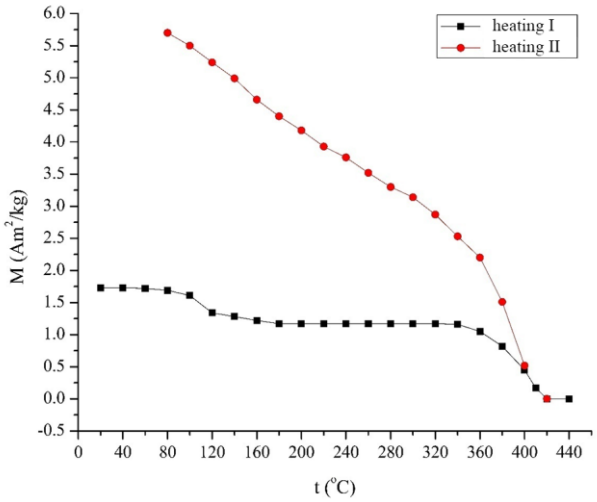

Fig. 7

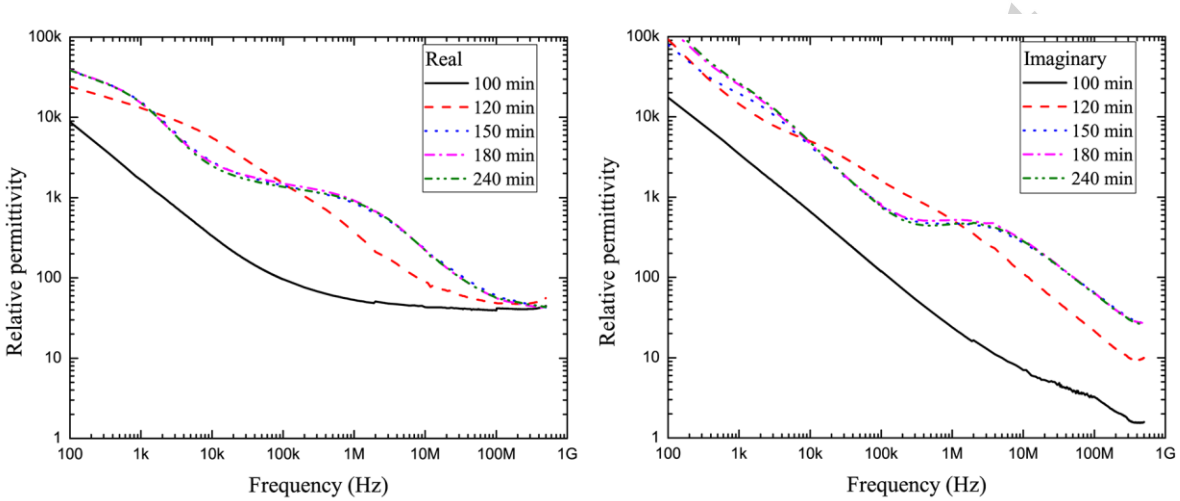

Fig. 8

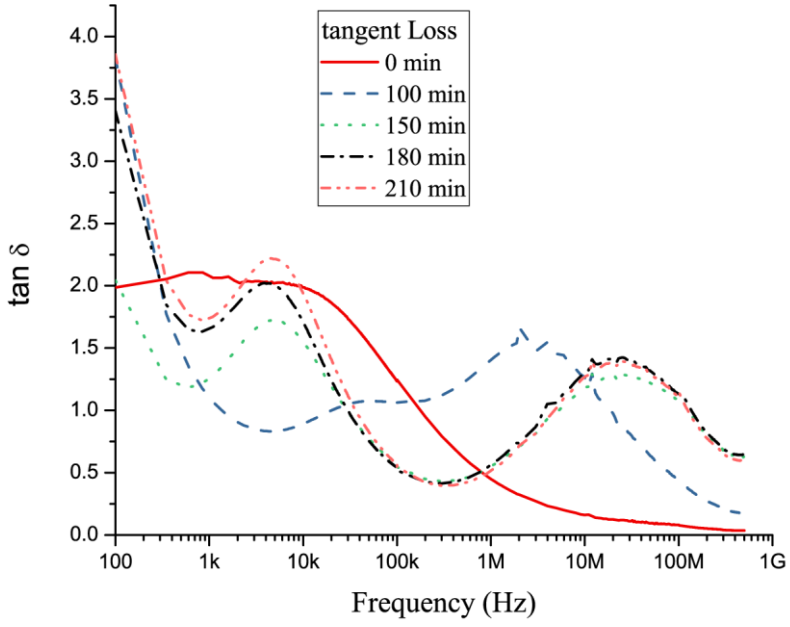

Fig. 9

Table 1. Results of Rietveld analysis (graphs included in the Supplement).

Sample	a	c	Size (nm)	Strain (%)	$O_{38}Ti_{1.26}Fe_{22.74}Ba_2$ (%mass)	$BaTiO_3$ (mass%)
100	5.88625	23.28505	2275	2.1	84.2	15.8
120	5.90449	23.21012	77	5.5	84.9	15.1
150	5.91424	23.22085	80	1.5	85.6	14.4
180	5.91213	23.20773	69	4.0	86.4	13.6
210	5.88672	23.23385	410	2.8	87.3	12.7
240	5.91802	23.21369	68	3.9	88.1	11.9